Imaging the Circumstellar Environments of Young Binaries in Southern Star-Forming Regions

Chris D. Koresko

Interferometry Science Center, Caltech, Pasadena, CA 91125

ABSTRACT

A sample of 14 pre-main sequence visual binary systems in southern star-forming regions were imaged at 2 μm with the Keck I telescope to search for tertiary companions, scattered-light disks, and compact nebulae at linear scales of 5–100 AU. Speckle holography was used to produce images with diffraction-limited resolution and high dynamic range, and photometry in four filters between J (1.25 μm) and L' (3.8 μm) was used to provide a diagnostic of the infrared excess. Of the 14 visual binary systems studied, 9 contain components which show evidence for resolved structure. Two of them (WSB 18 and B59-1) have well-resolved tertiary companions separated from the primary stars by $\sim$ 100 mas. The remainder are only marginally resolved at the diffraction limit of the telescope. Sz 116, AS 205, Elias 2-22, ESO Hα 282, and B59-2 each have one component which is marginally-resolved along one axis and unresolved on the perpendicular axis, consistent with tertiaries at separations between $\sim$ 6 and 40 mas. If all of these systems are hierarchical triples, then fully half of the nominal binaries in the sample are triple. The primaries in Elias 2-49 and WSB 71 are marginally resolved along all position angles, suggesting the presence of dust halos. No disks were unambiguously detected in the sample.

Subject headings: stars: pre-main-sequence — binaries: visual — circumstellar matter — methods: observational

1. Introduction

It has recently become clear that the great majority of the young low-mass stars in the nearest active star-forming regions (SFRs) are found in binary or multiple systems (Leinert et al. 1993; Ghez et al. 1993; Ghez et al. 1997). Although there is evidence that the mass in circumstellar material is smaller in binaries with separations $\lesssim$100 AU than in wider binaries or single stars (Jensen, Mathieu, & Fuller 1996), a majority of young binaries emit excess radiation at infrared or submillimeter wavelengths which is typically presumed to arise in dusty disks. If the presence of one or more stellar companions does not severely hamper a disk's ability to produce a planetary system, then binary and multiple systems probably contain the majority of the planets in the nearby SFRs.

At present, only two multiple-star systems are known to contain well-ordered, edge-on circumstellar disks visible because of their occlusion of the central star. The HK Tauri B and HV Tauri C disks exhibit a morphology much like that predicted by scattered-light models: A pair of bright lenslike reflection nebulae trace the upper and lower surfaces of the disk, while the dense region nearer the midplane is dark (Stapelfeldt et al. 1998; Koresko 1998; Monin & Bouvier 2000). There is no central point source seen in either the visible or near-infrared images. The near-infrared color of the HK Tauri B star+disk system is bluer than that of the primary star, presumably because the light we see is scattered by small particles.

A handful of visual binary companions to T Tauri stars are "infrared companions" (IRCs), objects unusually faint at visible wavelengths but bright in the infrared. The IRCs are mysterious because their spectral energy distributions show strong reddening and infrared excess reminiscent of stars at younger evolutionary phases than their

primaries (*e.g.,* Koresko, Herbst, & Leinert 1997). The structures seen in the two IRCs which have been resolved in published high-resolution images are not edge-on disk systems, but a diffuse and irregular nebula (Koresko et al. 1999) and a close double (Koresko 2000). Among the present sample, the companion to Elias 2-22 is known from previous observations (Chelli et al. 1988) to be an IRC.

Clearly, the circumstellar environments of young binary stars exhibit a range of phenomena which are accessible to modern imaging techniques. This paper describes the first results of an ongoing effort to characterize the circumstellar environments in a larger sample of young binary systems. The sources were chosen from the binaries detected in the visible-light imaging survey of Reipurth & Zinnecker (1993; hereafter RZ). They include all the binaries, with the exception of Sz 120, with separations between $1''.0$ and $3''.7$ and right ascensions between $16^h\ 06^m$ and $17^h\ 10^m$ (equinox 1950). This RA range includes all the RZ binaries in the Ophiuchus SFR, and several additional groups, for a total of 14 systems. The range of separations was chosen to avoid having the seeing-limited Point-Spread Functions (PSFs) overlap or fall off the edges of the detector. With one exception, the distances to the targets are given by RZ as 160 pc. Their physical separations are larger than 100 AU, so they are not expected to be strongly depleted of disk material via disk-companion interactions (Jensen, Mathieu, & Fuller 1996).

The sources are a somewhat mixed bag, consisting mainly of T Tauri stars but including at least one Herbig Ae/Be star (Elias 2-49) and a likely Post-T Tauri star (WSB 4). Many of the sources are well-studied, but a handful lack even published spectral types. Ten of the 14 systems are members of RZ's "systematic survey sample", which for the present purpose means that they were known to be members of dark clouds ~ 160 pc distant and are included in a list of young stars selected on the basis of a youth indicator such as near- or far-infrared excess or Ca II HK line emission. The remaining four systems are AS 205, both of whose components are Classical T Tauri stars (CTTS) (Prato et al. 1997); Elias 2-26, another CTTS (Martin et al. 1998); Elias 2-49, a Herbig Ae/Be star in Hillenbrand's Group I (Hillenbrand 1992);

and ESO Hα 282, about which little seems to be known beyond the fact that it is an emission-line source.

The 14 pre-main sequence binary systems were observed using speckle holography at near-infrared wavelengths $\sim 2\ \mu$m to produce diffraction-limited images with dynamic range of ~ 2000 at $0''.3$ from the star, which is much better than would have been possible with standard speckle imaging. The improved dynamic range is possible because the PSF is measured simultaneously with the science observations. Near-infrared photometry in the J, H, K, and L' bands was obtained the following night to measure the infrared excess of each component as a tracer of warm dust.

Two new tertiary companions with separations $\sim 0''.1$ were detected, and an additional 7 objects were found to be marginally resolved. Of these, 5 are extended along only one direction, which is consistent with the presence of a very close tertiary companion or a narrow extended structure such as a compact edge-on disk. The remaining two marginally-resolved objects were extended in all directions, which would be consistent with extended nebulosity but not with tertiary companions.

No new edge-on disks were unambiguously detected. It is known from theoretical models (*e.g.,* Wood et al. 1998) and from recent high-resolution images (*e.g.,* Burrows et al. 1996) that pre-main sequence circumstellar disks with fiducial mass distributions are readily detectable in visible-light or near-infrared images only when they are viewed along a line of sight close to the disk midplane. In this orientation, the direct radiation from the central star is blocked, making it possible to see the much fainter scattered light which traces the disk surface. The range of viewing angles over which the disk hides the star, and therefore the likelihood of detecting it if its orientation is random, depends on the disk's mass, radius, and flaring, and potentially on the degree to which the scattering dust has settled toward the midplane.

2. Observations

2.1. Holographic Imaging

The holography data were taken at the 10 m Keck 1 telescope on 1999 June 1 using the Near-Infrared Camera (NIRC; Matthews & Soifer 1994)

with the NIRC Image Converter (Matthews et al. 1996) to produce a magnified pixel spacing of 20 mas, approximately Nyquist-sampling the ~ 50 mas diffraction limit at the ~ 2 μm observing wavelength. The field of the 256×256 pixel detector was $5''.1$. The optical bandpass was set using either a standard K photometric filter, or, for stars which would saturate the detector in the K band, one of the narrower Ks or CH4 filters. The observations of each visual binary consisted of hundreds of frames with an integration time of 0.14 sec per frame. This short exposure time partially "froze" the atmospheric seeing, so that the raw PSF consisted of distinguishable speckles. The separations of these visual binaries were large enough compared to the $0''.5$ typical seeing that only a small fraction of the frames were rejected due to poor separation of the stars. The data for each visual binary system were divided into ~ 7 series of frames, with ~ 140 frames in each series. Series taken on blank sky were used to estimate the background and bias level. A journal of the holographic observations is given in Table 1.

Individual frames were calibrated by subtracting mean sky frames, dividing by flatfield images, and "fixing" bad pixels. A model was computed for the detector "bleed" signal which extended along the readout direction, as described in the NIRC manual, and this was subtracted from the calibrated frame. For each frame, a subframe centered on each of the stars was extracted, with one subframe being treated as the science measurement and the other serving as a measurement of the instantaneous point-spread function (PSF). The subframes were either 64×64 or 48×48 pixels in size; the smaller subframes were necessary for doubles whose separations were less than 64 pixels. The Fourier power spectra of the target and PSF subframes, and the cross-spectrum (*i.e.,* the Fourier transform of the cross-correlation) of the two subframes, were computed for each input frame. These quantities are meaningful within a roughly hexagonal region of the (u, v) plane containing spatial frequencies below the diffraction limit of the hexagonal Keck primary mirror.

The cross-spectrum, the target power, and the PSF power were averaged over the whole series of good frames. An averaged Fourier power spectrum and Fourier phase for the target, corrected for the distortions due to the atmosphere and the telescope, were reconstructed from them as follows: The power spectrum was estimated as the ratio of the average target power to the average PSF power, after removing a noise bias term from each. The phase was estimated as the phase of the averaged cross-spectrum. Uncertainties in the power spectrum and phase were estimated from the scatter between the averages computed for the ~ 7 series for each visual binary system. The PSF star in each binary was chosen arbitrarily, and the choice was reversed if it showed signs of resolved structure. In no system was there clear evidence that both stars were resolved, although in principle the technique would be insensitive to this if the morphologies of the two stars were sufficiently similar.

The reconstructed Fourier transforms were compared with models of single stars, double stars, and elliptical Gaussian halos. These choices clearly cannot span the range of all possible *astrophysical* models, but for targets which are only marginally resolved, they are sufficient to fit the features in the data. There is a degree of degeneracy in these model fits, in the sense that an unresolved star can always be fitted by a double-star model (with either zero separation or zero brightness ratio) or by a halo model (with zero axis lengths). Further, an object which is marginally resolved along only one axis can be fitted by either a double-star model or a halo model with a zero semiminor axis, since either model produces a power spectrum having a single broad stripe, and a nearly featureless phase, in the measured frequency range.

The comparisons with models were done separately for each series of frames. Only frequencies below that for which the median uncertainty rose to four times its low-frequency value at were used. For the double-star and halo models, the fitting was done 11 times for each series, with the starting values of the parameters varied randomly, and the fit with the smallest χ^2 value was chosen to represent that series. This was necessary because for some starting parameters the fitting routine became trapped in local minima in the χ^2 surface. The final parameter values for each model were the averages of the results for the series, and the quoted uncertainties are the standard deviations of the means of those results. These statistical uncertainties are likely to be optimistic be-

TABLE 1
HOLOGRAPHIC OBSERVATIONS

Object	Alt. Name	Region	D(pc)	Filter	Frames	Subframe Size
Sz 116	HBC 625	Lupus III	150	K	887	64
AS 205	HBC 254	B 40	?	CH4	941	64
WSB 4		Oph	160	K	1014	64
WSB 18		Oph	160	K	868	48
WSB 19		Oph	160	K	870	64
WSB 26	DoAr 23	Oph	160	K	848	48
Elias 2-22	DoAr 24E	Oph	160	Ks	716	64
WSB 35		Oph	160	K	864	64
Elias 2-26	ROX 15	Oph	160	K	857	64
WSB 71		Oph	160	K	813	64
Elias 2-49	HD 150193	Oph	160	Ks	384	48
ESO Hα 282		L 162	160	K	848	48
B59-1		B 59	160	K	822	64
B59-2		B 59	160	K	858	64

NOTE.— Holographic observations of the 14 pre-main sequence visual binary systems. The filters' center wavelengths and half-power bandwidths, measured in microns, are as follows: K (2.21 ± 0.42), Ks (2.16 ± 0.33), CH4 (2.27 ± 0.16). Distances are from Reipurth & Zinnecker 1993.

4

cause they do not include the effects of systematic biases. The estimation of physical parameters is rather delicate and easily affected by those biases, especially for the marginally-resolved sources.

For the marginally-resolved sources, the final misfit (χ^2 per degree of freedom) for the power spectrum was close to unity. The power spectra are more useful than the phases for marginally-resolved systems because the power spectra begin to show strong parameter-dependent structure at lower spatial frequencies than the phases do. On the other hand, the position angles derived from power spectra suffer from an ambiguity of 180 deg (*e.g.,* it is not possible to tell which star in a double is brighter). For the fully-resolved sources, which in the present sample are both primary-tertiary doubles, the fits to the power spectra tend to be poorer. This may be because the power spectra, being positive-definite, are susceptible to biases caused by zero-mean noise, while the phase tends to be unbiased by it. The phase fits also produce unambiguous position angles for resolved doubles. In summary, the phase data are more useful for resolved doubles, while the power spectra are more useful for marginally-resolved objects.

2.2.   Near-Infrared Photometry

The photometric fluxes of the target visual binary systems were crudely measured in the J, H, K, and L' filters at the Keck I telescope on 1999 June 2, by imaging them with NIRC. For the J, H, and K filters, subframes of 256×128 pixels were used with the Image Converter, while for the L' filter the Image Converter was removed and the subframe size was reduced to 32×32 or 64×32 pixels. These choices were driven largely by the need to read out the detector fast enough to avoid saturating it on the brighter stars or, at the longest wavelength, on the blank sky. The stars determined the peak signal levels in the J, H, and K filters, so the exposure times were adjusted between 68 msec and 4 sec, and no coadding was done. For the L' filter the frames consisted of 1000 coadds of 5 msec each. A total of 10 frames were taken on each target in each filter. Periodically, frames were obtained on blank sky to estimate the background level. SR3 served as a photometric standard for the J, H, and K filters, and HD 161793 was used for the L' filter.

The frames were calibrated in the usual way,

with sky-subtraction, flatfielding, and pixel-fixing. To derive the fluxes in the frames, each binary was fitted using a model in which the two stars were represented by circular Gaussians of adjustable size, intensity, and position. Although the Gaussians were not very good models for the PSFs, the fact that the PSF in each image was essentially identical for the two stars permitted the ratio of their brightnesses and the distance between them to be estimated accurately using this technique. The brightness ratios were combined with total flux measurements to derive the fluxes for the individual stars. At J, H, and K, these total fluxes were computed by summing the values of all pixels within 32 pixels of either star, after subtracting the background level estimated as the median value of all pixels at least 64 pixels away from either star. In the L' filter the total flux was simply the sum of all pixel-values, after subtraction of a background level. The photometric fluxes were calibrated in the usual way by comparison of these numbers with similar results on standard stars. No attempt was made to correct for the differences in airmass, as those corrections were found to be smaller than the statistical uncertainties. The final uncertainties in the magnitudes are approximately 0.2 mag.

Separations and position angles of the binaries were derived from the model fits in each filter. The platescale with IC out of the beam has been carefully measured by the Keck Observatory staff, and the pixel spacing is quoted in the instrument manual as $0''.1500$. By contrast, the $0''.02$ nominal platescale with the IC in is relatively uncertain. On the other hand, the measurements of the separation vectors taken with the smaller pixels are likely to be significantly more precise, in the sense of having smaller uncertainties if the platescale error is neglected. To take advantage of this, the assumed platescale in each of the J, H, and K bands was adjusted to make the mean separation for all the visual binaries (except for Sz 116, which was not measured in the L' filter, and Elias 2-49, which is anomalous as discussed below) equal to the mean separation in the IC-out L' images. The required IC-in pixel spacing of $0''.0207$ was consistent between the J, H, and K images. Similarly, the assumed orientation of the IC-in images was adjusted to make the mean difference between the IC-in and IC-out position angle measurements

vanish.

3. Results and Discussion

The results of the holographic imaging of the target binaries are summarized in Table 2, and the Fourier power spectra are displayed in Figure 1. The Table presents the values of χ^2 per degree of freedom (*i.e.,* per frequency element in the (u, v) plane) for unresolved-star, double-star, and halo models of the target in each of the 14 visual binary systems studied. For the two fully-resolved doubles, the fits were made to the Fourier phase, resulting in unambiguous position angle measurements, while for all other sources the fits were made to the power spectra. In the following discussion, a target is considered to be resolved if either the double-star or the halo model improves the χ^2 value by more than 0.5 compared to the unresolved-star model. This criterion provides a clean separation between the unresolved and extended targets.

The J,H,K,L' photometric measurements for the 14 holographic imaging targets are given in Table 3. Measurements of the separation vectors of their components, which are the averages of those measured at J, H, and K with the corrected platescale, are included in the table. The brightness ratios for the visual binaries are plotted in Figure 2.

Out of the 14 visual binary systems (nominally 28 stars) observed, two are found to be well-resolved doubles, 5 to be marginally resolved along a single axis (consistent both with doubles with separations less than the diffraction limit, or with elongated halos), and two were marginally-resolved along all axes. The results for the individual resolved and marginally-resolved sources are discussed below.

3.1. Fully-Resolved Primary-Tertiary Pairs

Two systems (WSB 18 and B59-1) have well-resolved tertiary companions separated from their primaries by $\sim 0''.1$. Models were fitted to their Fourier phases in order to derive the brightness ratio R, separation ρ, and position angle θ of the primary-tertiary pairs. The results are given in Table 4.

The presence of a tertiary companion to the primary in WSB 18 is noteworthy in light of the study by Brandner & Zinnecker (1997), in which the primary appeared somewhat more luminous than would have been predicted for a single star with its M2 spectral type and the 5×10^6 yr age derived by comparing the secondary to the theoretical pre-main sequence tracks of D'Antona & Mazzitelli (1994). It is natural to suggest that the tertiary companion is responsible for the excess luminosity, and its detection strengthens the conclusion reached by Brandner & Zinnecker (1997) that the components of the binaries in their sample are coeval.

The projected separations of these primary-tertiary systems correspond to ~ 16 AU at 160 pc. Assuming that the true separations are not much larger, that the mass of each close pair is ~ 0.6 M$_\odot$, and that the orbits are circular, results in an estimate of $\sim 10^2$ yr for their orbital periods. The systems should rotate by ~ 4 deg yr^{-1}, making their orbital motion readily detectable from one year to the next.

3.2. Marginally-Resolved Sources

As discussed above, the nature of the 7 marginally resolved targets is somewhat ambiguous. Five of them appear to be extended along only one axis, making them consistent with both the double-star model (the double having a separation below the diffraction limit) and the halo model (the minor axis being much smaller than the major axis). In these cases, the double-star model is preferred for its astrophysical simplicity, although it may be possible to produce an elongated halo of the observed size by a suitable arrangement of circumstellar material such the inner regions of a nearly edge-on disk. The results of fitting the double-star model to these sources are included in Table 4.

The power spectrum of the Sz 116 secondary is consistent with a double whose separation is just below the diffraction limit. The best-fit model gives a projected separation of 40 mas, corresponding to 6 AU at 160 pc, making this the widest of the potential marginally-resolved doubles in the sample. The secondaries in AS 205, Elias 2-22, ESO Hα 282, and the primary in B59-2 also have asymmetrical power spectra consistent with the presence of tertiary companions with sep-
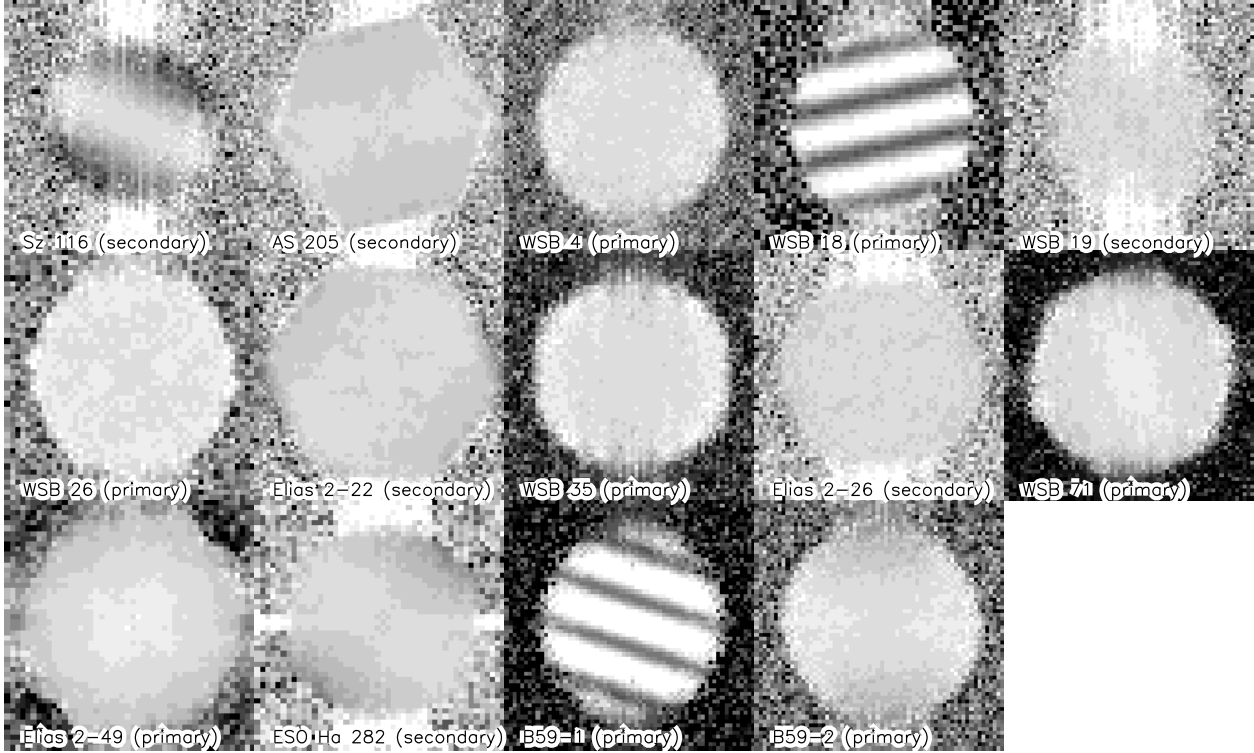
Fig. 1.— Reconstructed visibility amplitudes for the target components in the 14 visual binaries, displayed with the zero frequency at the center of each plot, and in the orientation natural to the detector. The measured amplitudes extend from the zero-frequency point to something close to the diffraction limit of the Keck primary mirror, whose hexagonal shape is visible in the data on the brighter stars. At high frequencies detector noise produces stripes parallel to the horizontal or vertical axes. The striped structure consistent with the presence of close tertiary companions is obvious in Sz 116, WSB 18, and B59-1. Closer inspection reveals similar (but broader) central stripes in AS 205, ESO Hα 282, B59-2, and possibly in Elias 2-22. The amplitudes of WSB 71 and Elias 2-49 decrease in all directions, which is inconsistent with a tertiary-star model.

TABLE 2

SUMMARY OF HOLOGRAPHIC IMAGING RESULTS

Object	Fit To	Target	χ_u^2	χ_d^2	χ_h^2	Comment
Sz 116	power	sec	9.4	1.5	1.5	1
AS 205	power	sec	4.7	1.1	1.2	1
WSB 4	power	pri	1.1	1.1	1.1	4
WSB 18	phase	pri	96	1.2	96	2
WSB 19	power	sec	1.6	1.6	1.6	4
WSB 26	power	pri	1.1	1.1	1.1	4
Elias 2-22	power	sec	1.9	1.1	1.1	1,5
WSB 35	power	pri	1.4	1.4	1.4	4
Elias 2-26	power	sec	1.1	1.1	1.1	4
WSB 71	power	pri	2.1	1.5	1.3	3
Elias 2-49	power	pri	3.6	2.0	1.0	3
ESO Hα 282	power	sec	6.6	1.5	1.5	1
B59-1	phase	pri	47	1.2	47	2
B59-2	power	pri	2.3	1.1	1.1	1

NOTE.— Fits were made to the Fourier phase data for the two fully-resolved doubles, and to the power spectra for all other targets. χ_u^2, χ_s^2, and χ_h^2 are the χ^2 per degree of freedom for the unresolved, double, and halo models, respectively. The comment numbers are: (1) Marginally-resolved, consistent with a tertiary or a halo. (2) Fully-resolved double. (3) Marginally-resolved, consistent with a halo but not a tertiary. (4) No evidence of resolved structure (5) Infrared Companion. This system is also known as DoAr 24E.

TABLE 3

INFRARED PHOTOMETRY AND SEEING-LIMITED IMAGING

Object	J_{pri}	H_{pri}	K_{pri}	L'_{pri}	J_{sec}	H_{sec}	K_{sec}	L'_{sec}	Sep ($''$)	PA (deg)
Sz 116	10.5	9.5	9.9		11.1	10.4	10.4		1.65	26.5
As 205	8.3	6.9	6.2	5.4	8.8	7.5	7.0	5.9	1.34	211.3
WSB 4	11.6	11.0	10.9	10.1	11.9	11.2	10.6	9.1	2.84	128.5
WSB 18	11.1	10.1	10.0	8.9	11.8	10.8	10.4	9.0	1.08	80.4
WSB 19	10.8	9.7	9.6	8.4	11.5	10.5	10.4	9.3	1.53	260.7
WSB 26	10.9	9.9	9.6	8.5	11.4	10.2	9.7	8.1	1.15	23.8
Elias 2-22	8.7	7.5	7.1	6.1	11.6	9.1	7.7	5.6	2.05	148.6
WSB 35	10.8	9.7	9.3	8.0	11.5	10.7	10.6	9.9	2.29	130.3
Elias 2-26	10.5	8.8	8.4	7.2	11.9	10.2	9.6	8.3	1.44	67.0
WSB 71	10.1	8.8	8.0	6.2	11.0	10.1	9.9	9.2	3.56	35.0
Elias 2-49	7.1	6.4	5.9	5.2	8.5	7.8	7.8	6.8	1.09	221.7
ESO Hα 282	9.8	8.6	7.8	6.8	11.1	10.1	9.5	8.6	1.03	251.8
B59-1	11.8	9.8	9.0	7.5	13.1	11.5	11.0	10.2	3.44	109.3
B59-2	10.0	9.3	9.3	8.9	11.3	10.4	10.1	8.9	3.11	207.0

NOTE.— Near-infrared magnitudes and separation vectors for the holographic target binaries, based on corrected JHK measurements as described in the text. The position angles are computed for vectors extending from the brighter to the fainter component in the J filter. They are measured in degrees east of North. The estimated photometric uncertainties are typically 0.2 mag, and the scatter between the J, H, and K separation vector measurements for a given star is typically smaller than $0''.01$ in separation and 0.2 deg in position angle.

TABLE 4
DOUBLE-STAR FITS

Object	θ (deg)	R	Sep (mas)
Sz 116	$143.3 \pm .4$	$0.37 \pm .01$	$36.9 \pm .4$
AS 205	101 ± 1	$1 \pm .003$	$8.5 \pm .4$
WSB 18	$339.55 \pm .05$	$0.505 \pm .001$	$100.4 \pm .1$
Elias 2-22	44 ± 3	$0.98 \pm .001$	$5.6 \pm .2$
ESO Hα 282	$16.7 \pm .6$	$0.78 \pm .02$	$12.8 \pm .1$
B59-1	$218.9 \pm .1$	$0.49 \pm .002$	$106.7 \pm .1$
B59-2	$113.5 \pm .5$	$0.91 \pm .05$	$12.2 \pm .1$

NOTE.— Double-star fitting parameters for the Fourier phase data on the two objects with clearly-resolved tertiary companions, and fits to the Fourier power spectra of the five objects which exhibit marginally-resolved structure which consistent with the double-star model. In the latter cases, the R (brightness ratio) and ρ (separation) values must be considered representative of a class of possible models, and the position angle (θ) values are ambiguous by 180 deg. The errorbars quoted here are derived from the standard deviation of the mean derived from the scatter among fits to ~ 7 series of ~ 140 frames each. They do not include any potential contributions from uncertainties in the platescale or orientation of the camera, or noise biases. They are very optimistic, especially for the marginally-resolved objects.

TABLE 5
GAUSSIAN HALO FITS TO MULTIAXIAL POWER SPECTRA

Object	comp	Fit to	θ (deg)	a (mas)	b (mas)
WSB 71	pri	power	8 ± 3	64 ± 1	50 ± 1
Elias 2-49	pri	power	116 ± 3	54 ± 1	45 ± 1

NOTE.— Gaussian-halo fitting parameters for the Fourier power data on the two objects which are marginally resolved but not consistent with the double-star model. The parameters are the position angle of the major axis and the lengths of the semimajor and semiminor axes.

arations ranging from only 6 to 13 mas, well below the diffraction limit. If the structures seen in these targets do reflect tertiary companions, their periods would be only $\sim 1 - 20$ yr. For these marginally-resolved objects, followup holographic observations to search for significant changes in the position angles of their extended structures would provide a good test of the tertiary-star interpretation.

The primary components in Elias 2-49 and WSB 71 are marginally-resolved but inconsistent with the double-star model because there is no position angle along which the power spectra do not decrease with frequency. In these objects the χ^2 is lower for the halo model than for the double-star model. The data are insufficient to determine the morphology of these sources in any detail, and it may be much more complex than a simple Gaussian halo. The marginally-resolved primaries in these systems are much redder than the unresolved secondaries (see Figure 2), which is not surprising if they are surrounded by dust envelopes, provided that the overall flux is not dominated by scattering. These sources merit followup observations at shorter wavelengths, *e.g.,* visible-light imaging with the *Hubble Space Telescope*, to search for extended, low surface brightness scattered light to which the present holographic observations are insensitive.

3.3. Wavelength Dependence of Visual Binary Separation Vectors

If a star has a close companion with a significantly different infrared color, or if it is surrounded by an asymmetrical halo of non-gray dust, then its photocenter will be wavelength-dependent. A comparison between the separation vectors measured for a visual binary over a range of wavelengths can potentially detect this effect. The RMS scatter in the differences between the IC-in and IC-out separation values for the binaries, excluding Sz 116 (which was not measured at L') and Elias 2-49, is $0''.014$. This gives an indication of the precision of the individual separation measurements. For Elias 2-49 the separation decreases with wavelength from $1''.09$ at J to $0''.97$ at L', a change which is much larger change than the estimated precision and suggestively similar to the estimated Gaussian size of the halo surrounding the primary star. Deeper high-resolution images of

this system at visible or near-infrared wavelengths would be useful to reveal the structure of the circumstellar material. Interestingly, WSB 71, the other system which appears to have a halo around its primary, has a separation which is not dependent on wavelength between the J and L' bands.

3.4. The Density of Tertiary Companions

If one assumes that all five marginally-resolved sources which are compatible with doubles do have physical tertiary companions at the separations derived from the model fits, then fully half of the nominal visual binaries in the sample are actually hierarchical triples. This perhaps surprising result is discussed below.

The angular surface density $\Sigma(\theta)$ of companions to young stars in the Taurus, Ophiuchus, and Orion star-forming regions was computed by Simon (1997) for companion separations θ as small as $0''.01$. In the "binary regime" in which θ is small enough that Σ is dominated by bound objects, the surface density in all three clusters was found to be $\Sigma(\theta) \propto \theta^{-b}$, where b is close to 2.0. A similar conclusion was reached for an X-ray selected sample of Taurus stars by Kohler & Leinert (1998; hereafter KL98) for separations between $0''.13$ and $13''$. The robustness of this result is impressive in light of range of physical conditions spanned by the three SFRs.

Suppose that this result applies within the present sample of visual binaries for tertiaries at separations small compared to the visual binary separation. This cannot be strictly true, both because the sample is *statistically* biased by the presence of the visual companions and because the companions' gravitational influence restricts the range of separations for which a stable tertiary orbit may exist, but given the large ratio of the observed outer to inner separations and the steepness of the density function, it may not be terribly wrong. The orbital stability restriction has been estimated by Harrington (1972) and depends on the inclination of the inner orbit relative to the outer orbit, the eccentricity of the outer orbit, and the mass ratios of the components, but for an outer-orbit eccentricity of 0.5 and components of similar mass it requires the major axis of the outer orbit to be approximately a factor of 10 larger than
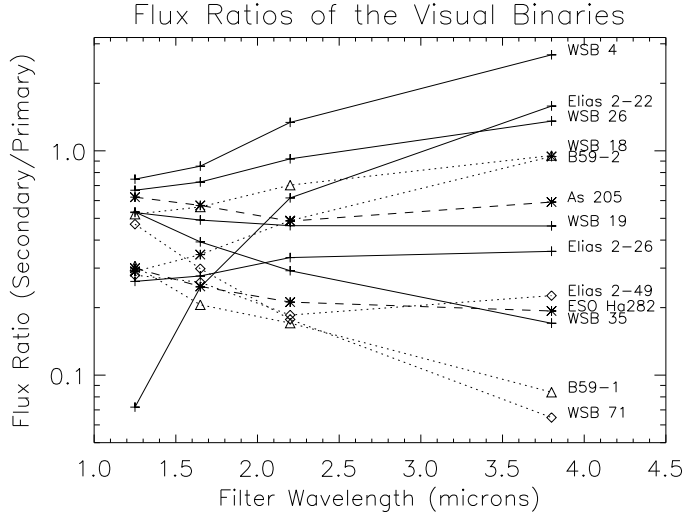
Fig. 2.— The brightness ratios for the visual binaries in the sample, estimated by fitting the seeing-limited images with models consisting of a pair of circular Gaussians, for the four filters. Sz 116 is not included on the plot because the L' measurement on it was not successful.
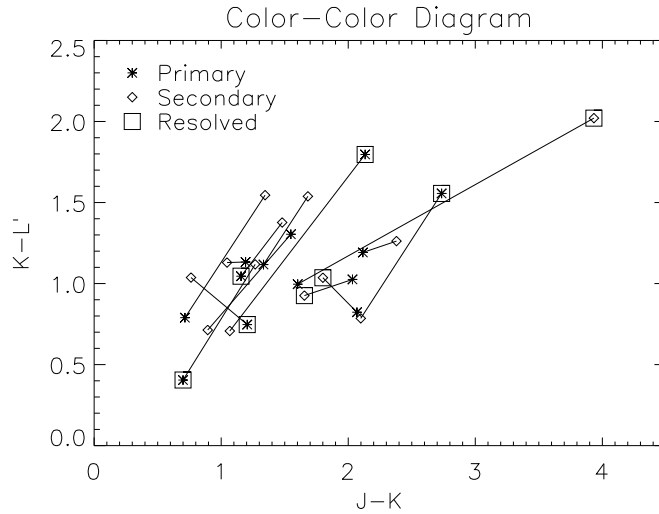

Fig. 3.— The near-infrared colors of the components of the visual binary systems in the sample are plotted with symbols indicating their rank (*i.e.,* whether they are primary or secondary stars). Symbols for the components of each system are joined by a line. A box surrounding a symbol indicates that it was marginally or fully resolved by the holographic observations. The data reveal no clear correlation between brightness, color, or structure.

12

that of the inner orbit. The average projected separation of the visual binaries in the present sample is $2''$, so according to the Harrington criterion with the assumed parameters, and neglecting the effects of projection onto the plane of the sky, the systems on average should permit tertiary companions with separations no larger than about 200 mas. Normalizing Σ to produce the number of companions observed by KL98 within the range of radii to which their observations were sensitive, and integrating over an annulus extending from the approximate detection limit of 5 mas to the stability cutoff at 200 mas, leads to a prediction that 11 tertiaries should be found among the 28 primary and secondary stars in the sample. Given the small sample size, the crudeness of the above approximations, and the possibility that some additional tertiary companions were missed, this is consistent with the 7 detected here.

3.5.   Infrared Brightness Ratios

The brightness ratios for the target visual binaries measured in all four filters, plotted against the filter wavelengths in Figure 2, show no clear tendency for the primary star in a visual binary to be redder than the secondary. Such a tendency would be manifested as a generally negative slope in the brightness-ratio curves. This contrasts with the result for the sample of Taurus visual binary TTS observed by Moneti & Zinnecker (1991), in which the primary stars were redder than the secondaries. An examination of the color-color plot in Figure 3 shows no clear correlations between the colors of the visual binary components, their structure in the holographic observations, or their relative brightness.

4.   Conclusions

The present study is among the first to probe a sample of pre-main sequence visual binary systems with this combination of high resolution and dynamic range in the near-infrared. The results are not very consistent with the naive expectations that motivated it. More than half of the systems contain resolved or marginally-resolved components. Two tertiary companions were clearly resolved at ~ 100 mas separations from their primaries, and tertiaries at separations below the diffraction limit are likely to account for the struc-

ture seen in all but two of the marginally-resolved stars, including the infrared companion (IRC) in Elias 2-22. Followup observations to search for orbital motion would be useful. The presence of such a large number of tertiary companions would make it necessary to search binary systems carefully before attempting to use them to test pre-main sequence tracks, since the light of an undetected tertiary will make a star appear younger and more luminous that it is. Two stars showed extended structure which appears to be due to the presence of dust halos rather than tertiary companions, and one of these (Elias 2-49) has a separation which decreases with wavelength. Strikingly absent is a clear detection of an edge-on circumstellar disk in any of the binaries in the sample.

REFERENCES

Brandner, W. & Zinnecker, H. 1997, A&A, 321, 220

Burrows, C.J., Stapelfeldt, K.R., Watson, A.M., Krist, J.E., Ballester, G.E., Clarke, J.T., Crisp, D., Gallagher, J.S., III, Griffiths, R.E., Hester, Jeff, Hoessel, J.G., Holtzman, J.A., Mould, J.R., Scowen, P.A., Trauger, J.T., & Westphal, J.A. 1996, ApJ, 473, 437

Chelli, A., Cruz-Gonzalez, I., Zinnecker, H., Carrasco, L., & Perrier, C. 1988, A&A, 207, 46

Close, L. M., Dutrey, A., Roddier, F., Guilloteau, S., Roddier, C., Northcott, M., Menard, F., Duvert, G., Graves, J. E., & Potter, D. 1998, ApJ, 499, 883

D'Antona, F. & Mazzitelli, I. 1994, ApJS, 90, 467

Ghez, A.M., Neugebauer, G., & Matthews, K. 1993, AJ, 106, 2005

Ghez, A.M., McCarthy, D.W., Patience, J.L., & Beck, T.L 1997, ApJ, 481, 378

Harrington, R.S. 1972, Celest. Mech. 6, 322

Hillenbrand, L.A., Strom, S.E., Vrba, F.J., & Keene, J. 1992, ApJ, 397, 613

Jensen, E.L.N., Mathieu, R.D., & Fuller, G.A. 1996, ApJ, 458, 312

Kohler, R. & Leinert, Ch. 1998, å, 331, 977

Koresko, C.D., Herbst, T.M., & Leinert, Ch. 1997, ApJ, 480, 741

Koresko, C.D. 1998, ApJ, 507, 145

Koresko, C.D., Blake, G.A., Brown, M.E., Sargent, A.I., & Koerner, D.W. 1999, ApJ, 525, 49

Koresko, C.D. 2000, ApJ, 531, 147

Leinert, Ch., Zinnecker, H., Weitzel, N., Christou, J., Ridgway, S. T., Jameson, R., Haas, M., & Lenzen, R. 1993, A&A, 278, 129

Martin, E.L., Montmerle, T., Gregorio-Hetem, J., Casanova, S. 1998 MNRAS, 300, 733

Matthews, K. & Soifer, B.T. 1994, Infrared Astronomy with Arrays: The Next Generation. I. McLean, Ed. (Dordrecht: Kluwer Acadameic Publishers), 239

Matthews, K., Ghez, A.M., Weinberger, A.J., & Neugebauer, G. 1996, PASP, 108, 615

Moneti, A.; Zinnecker, H. 1991, A&A, 242, 428

Monin, J.-L. & Bouvier, J. 2000, A&A, 356, L75

Prato, L. & Simon, M. 1997, ApJ, 474, 455

Reipurth, B. & Zinnecker, H. 1993, A&A, 278, 81 (RZ)

Simon 1997, ApJ, 482, 81

Stapelfeldt, K.R., Krist, J.E., Menard, F., Bouvier, J., Padgett, D.L., & Burrows, C.J. 1998, ApJ, 502, 65

Wilking, Bruce A.; Schwartz, Richard D.; Blackwell, James H. 1987, AJ, 94, 106

Wood, K., Kenyon, S.J., Whitney, B., & Turnbull, M. 1998, ApJ, 497, 404